

This is an Accepted Manuscript version of the following article, accepted for publication in:


B. Arribas, G. Almandoz, A. Egea, J. Poza and I. Iturbe, "Analysis of Multiphase Permanent Magnet Motors via Space-Harmonic Model," *2024 International Conference on Electrical Machines (ICEM)*, Torino, Italy, 2024, pp. 1-7.

DOI: <https://doi.org/10.1109/ICEM60801.2024.10700420>


© 2024 IEEE. Personal use of this material is permitted. Permission from IEEE must be obtained for all other uses, in any current or future media, including reprinting/republishing this material for advertising or promotional purposes, creating new collective works, for resale or redistribution to servers or lists, or reuse of any copyrighted component of this work in other works.

Analysis of Multiphase Permanent Magnet Motors via Space-Harmonic Model


Beñat Arribas

Electronics and Computing Department
Mondragon Unibertsitatea
Arrasate, Spain
barribas@mondragon.edu 


Gaizka Almandoz

Electronics and Computing Department
Mondragon Unibertsitatea
Arrasate, Spain
galmandoz@mondragon.edu 


Aritz Egea

Electronics and Computing Department
Mondragon Unibertsitatea
Arrasate, Spain
aegea@mondragon.edu 

Javier Poza

Electronics and Computing Department
Mondragon Unibertsitatea
Arrasate, Spain
jpoza@mondragon.edu 

Ion Iturbe

Electronics and Computing Department
Mondragon Unibertsitatea
Arrasate, Spain
iiturbeb@mondragon.edu 

Abstract—Multiphase permanent magnet motors are gaining popularity thanks to their advantages, which include reduced torque ripple, enhanced torque capability, and fault tolerance. However, their modelling and control is more complex. Different harmonics in multiphase motors are separated in different orthogonal planes, each one having a different inductance value. This has different implications in airgap flux and torque generation. In this work, we present a space-harmonic model to analyse the torque production and the inductances in multiphase motors. This contributes to understand the interaction between different harmonics and their implication on the motor characteristics, which can be helpful for the motor design. To further verify the results, a three-phase and a dual three-phase motor are compared with finite element models. The case study confirms the results obtained from the space-harmonic model.

Index Terms—multiphase, space-harmonic, modelling, Current Harmonic Injection (CHI), inductance, torque

I. INTRODUCTION

The multiphase permanent magnet motor is gaining popularity in many sectors such as automotive, thanks to its numerous advantages including reduced torque ripple, enhanced torque capability, and fault tolerance [1]. Despite its advantages, multiphase motor modelling is more complex than that of their three-phase counterparts [2].

Unlike in 3-phase motors, where time-varying variables can be represented in a single plane (usually called $\alpha\beta$ plane), multiphase motors have more than one orthogonal plane, each one containing harmonics of a specific sequence [3]. Therefore, it is necessary to characterise each plane, given their different inductance values. In [4] and [5], an algorithm to get the inductance in each plane is proposed and experimentally verified.

The winding function theory has also been used to compute the inductances in multiphase windings. In [6], it was used to

calculate the inductances of surface permanent magnet motors. In [7], it was combined with Finite Element Method (FEM) to make an accurate model taking into account stator and rotor reluctance.

Space-harmonic models based on winding function theory were used to analyse torque production in switched flux permanent magnet [8], surface permanent magnet [9], and axial permanent magnet [10] motors. In [11], the time-harmonics and space-harmonics were analysed in a multiphase induction motor using a space-harmonic model.

In the literature, the winding function theory has been used in multiphase motors to calculate the inductances of different planes. Moreover, the airgap flux generation has been analysed with space-harmonic models. Yet, to the best of our knowledge, the models have not been used to analyse in depth the interaction of the different harmonics so as in this article.

The aim of this paper is to deepen the understanding of the different harmonic planes, inductances and torque generation in multiphase motors thanks to a space-harmonic model. Different design variables are taken into account (number of phases, winding configurations, magnet spans, current waveforms, and so on), whose effect in the inductances and torque generation is analysed in depth. This can be helpful in the motor design stage. The model was validated with a case study of a three-phase and a Dual Three-Phase (DTP) motors with FEM.

II. ASSUMPTIONS AND NOTATION

As the objective of the space-harmonic model is to understand how the coupling between different harmonics affects the inductances and torque ripple, several assumptions are made:

- Slotless stator and rotor: The stator and the rotor are considered flat, this is, the effect of stator teeth and rotor saliency is disregarded.
- Infinite stator and rotor core permeability: The airgap defines the permeance of the magnetic circuit.

This work was supported in part by the Basque Government under: ELKARTEK reference KK-2023/00091, and Non-Doctoral Research Staff Training Programme grants PRE-2022-1-0137 and PRE-2023-2-0287

- No flux leakages: All the flux goes through stator core, rotor core and coils.
- Unitary pole pairs and periodicity: The analysis is performed in the entire perimeter of the air gap.
- Disregarded airgap length: Stator inner, rotor outer and airgap diameters are considered the same (D_g). Airgap (g) is only used for permeance calculation.

When defining the magnitudes (e.g. magnitude X represented in (1)), subscripts are used to refer to the location of the magnitude (e.g. phase ph or airgap g), and superscripts are used to refer to the cause of the magnitude (e.g. phase ph , whole stator armature s or permanent magnets pm).

$$X_{\square \rightarrow \square}^{\square \rightarrow \square} \quad (1)$$

$\square \rightarrow \square$ Magnitude cause
 $\square \rightarrow \square$ Magnitude location

On the other hand, the mechanical angles in the stator (θ_s) and in the rotor (θ_r) are related by (2). The analysis is performed in the stationary reference frame (variables are represented with respect to the stator position θ_s).

$$\theta_r = \theta_s - \Omega t \quad (2)$$

III. SPACE-HARMONIC MODEL

Fig. 1 shows the process of calculating the torque and inductance expressions with the space-harmonic model, which are described in detail below.

A. Torque production

The winding function of phase ph depends on the stator angular position. It is expressed as in (3),

$$M_{ph}(\theta_s) = \sum_{n=-\infty}^{\infty} \frac{1}{2} \hat{M}_n e^{jn(\theta_s - \theta_{0,ph})} \quad (3)$$

where \hat{M}_n and $\theta_{0,ph}$ are the n^{th} winding function harmonic amplitude and phase shift of the phase winding with respect to the reference phase.

Conversely, the flux density generated in the airgap by the permanent magnets is a function of time and position, and is given by (4),

$$B_g^{pm}(\theta_s, t) = \sum_{p=-\infty}^{\infty} \frac{1}{2} \hat{B}_{g_p} e^{jp(\theta_s - \Omega t)} \quad (4)$$

where \hat{B}_{g_p} is the p^{th} harmonic amplitude of magnetic flux density generated by the permanent magnets in the airgap.

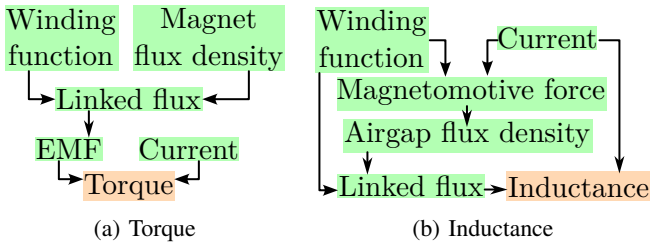


Fig. 1: Torque and inductance calculation process.

To compute the permanent magnet flux linked in each phase, the flux density in the airgap must be multiplied by the corresponding winding function and integrated across the airgap area. This is written in (5),

$$\Psi_{ph}^{pm}(t) = \oint_{S_g} M_{ph}(\theta_s) \cdot B_g^{pm}(\theta_s, t) \cdot dS \quad (5)$$

where S_g is the airgap area. The differential operator of the area is expressed in (6) as a function of the stator position θ_s ,

$$dS_g = \frac{L_s D_g}{2} d\theta_s \quad (6)$$

where L_s and D_g are the length of the stator and the diameter of the air gap, respectively.

Thus, by replacing (6) in (5), (7) is obtained.

$$\begin{aligned} \Psi_{ph}^{pm}(t) &= \frac{L_s D_g}{2} \int_0^{2\pi} M_{ph}(\theta_s) \cdot B_g^{pm}(\theta_s, t) \cdot d\theta_s = \\ &= \frac{L_s D_g}{8} \sum_{[n,p]=-\infty}^{\infty} \hat{M}_n \hat{B}_{g_p} e^{-j(n\theta_{0,ph} + p\Omega t)} \int_0^{2\pi} e^{j(n+p)\theta_s} d\theta_s \end{aligned} \quad (7)$$

To obtain a non-zero value in the integration in (7), $p = -n$ must be fulfilled. Applying the mentioned equality and solving the integral results in (8).

$$\Psi_{ph}^{pm}(t) = \frac{L_s D_g \pi}{4} \sum_{n=-\infty}^{\infty} \hat{M}_n \hat{B}_{g_n} e^{jn(\Omega t - \theta_{0,ph})} \quad (8)$$

Equation (8) shows that permanent magnet flux is linked in the cases that the order of winding factor and permanent magnet flux harmonics are the same. Other winding factor harmonics do not have an effect on permanent magnet flux linkage.

The back electromotive force (EMF) in each phase is the derivative of the linked magnet flux over time as shown in (9).

$$EMF_{ph}(t) = - \frac{d\Psi_{ph}^{pm}(t)}{dt} \quad (9)$$

If the permanent magnet linked flux in (8) is substituted in (9) and developed, the representation of the phase EMF in (10) is achieved.

$$EMF_{ph}(t) = \frac{L_s D_g \Omega \pi}{4} \sum_{n=-\infty}^{\infty} n \hat{M}_n \hat{B}_{g_n} e^{jn(\Omega t - \theta_{0,ph})} e^{j\frac{3\pi}{2}} \quad (10)$$

Furthermore, the phase current of phase ph is time dependent and is given by (11),

$$I_{ph}(t) = \sum_{k=-\infty}^{\infty} \frac{1}{2} \hat{I}_k e^{jk(\Omega t - \theta_{0,ph} + \lambda_k)} \quad (11)$$

where \hat{I}_k and λ_k are the amplitude of k^{th} current harmonic and its angle, respectively.

When it comes to the torque produced by the interaction between the flux generated by permanent magnets and the

armature winding, one way to calculate it is to calculate the electromagnetic power, by multiplying the back electromotive force (EMF) and the armature currents, and then dividing it by mechanical speed as in (12).

$$T_{em}^{pm-ph}(t) = \frac{EMF_{ph}(t) \cdot I_{ph}(t)}{\Omega} \quad (12)$$

Substituting (10) and (11) into (12) and developing it, (13) is obtained, which is the expression for the torque generated by a given phase.

$$T_{em}^{pm-ph}(t) = \frac{L_s D_g \pi}{8} \cdot \sum_{[k,n]=-\infty}^{\infty} n \hat{M}_n \hat{B}_{g_n} \hat{I}_k e^{j(n+k)(\Omega t - \theta_{0,ph})} e^{j(\frac{3\pi}{2} + k\lambda_k)} \quad (13)$$

To calculate the overall torque, the sum of torque of all phases must be computed by substituting θ_0 of each phase in (13) and summing the torque values in all phases, obtaining (14).

$$T_{em}^{pm-s}(t) = \frac{L_s D_g \pi}{8} \sum_{\theta_0} \sum_{[k,n]=-\infty}^{\infty} n \hat{M}_n \hat{B}_{g_n} \hat{I}_k \cdot e^{j(n+k)\Omega t} e^{-j(n+k)\theta_0} e^{j(\frac{3\pi}{2} + k\lambda_k)} \quad (14)$$

B. Inductances

The MagnetoMotive Force (MMF) generated by each phase winding is the product between the winding function and the current in the corresponding phase. This relationship is represented in (15), which is developed by substituting (11) and (3), obtaining (16).

$$MMF^{ph}(\theta_s, t) = M_{ph}(\theta_s) \cdot I_{ph}(t) \quad (15)$$

$$MMF^{ph}(\theta_s, t) = \frac{1}{4} \sum_{[n,k]=-\infty}^{\infty} \hat{M}_n \hat{I}_k e^{j(n\theta_s + k\Omega t + k\lambda_k)} e^{-j(n+k)\theta_{0,ph}} \quad (16)$$

Once the MMF generated by each phase is calculated, the overall MMF generated by the armature winding is calculated in (17), which is obtained by adding all phase magnetomotive forces as in (17).

$$MMF^s(\theta_s, t) = \sum_{\theta_0} MMF^{ph}(\theta_s, t) = \frac{1}{4} \sum_{\theta_0} \sum_{[n,k]=-\infty}^{\infty} \hat{M}_n \hat{I}_k e^{j(n\theta_s + k\Omega t + k\lambda_k)} e^{-j(n+k)\theta_0} \quad (17)$$

Starting from the MMF, the magnetic flux density in the airgap generated by a given phase is calculated. This is the product between the magnetomotive force generated by the phase and the permeance of the circuit as shown in (18),

$$B_g^{ph}(\theta_s, t) = \frac{MMF^{ph}(\theta_s, t) \cdot \Lambda_g(\theta_s)}{S_g} \quad (18)$$

where Λ_g is the permeance of the airgap in each airgap point. The airgap permeance is calculated in (19) and developed by substituting (6),

$$\Lambda_g = \frac{\mu_0}{g} S_g \quad (19)$$

being $\mu_0 = 4\pi \cdot 10^{-7}$ H/m the air permeability and g the length of the airgap. By substituting (16) and (19) in (18), the airgap flux density generated by a single stator coil is shown in (20).

$$B_g^{ph}(\theta_s, t) = \frac{1}{4} \frac{\mu_0}{g} \sum_{[n,k]=-\infty}^{\infty} \hat{M}_n \hat{I}_k e^{j(n\theta_s + k\Omega t + k\lambda_k)} e^{-j(n+k)\theta_{0,ph}} \quad (20)$$

The same way, magnetic flux density generated by the whole stator armature can be obtained by substituting the MMF generated by the whole armature (17) in (18), resulting in (21).

$$B_g^s(\theta_s, t) = \frac{MMF^s(\theta_s, t) \cdot \Lambda_g(\theta_s)}{S_g} = \frac{1}{4} \frac{\mu_0}{g} \sum_{\theta_0} \sum_{[n,k]=-\infty}^{\infty} \hat{M}_n \hat{I}_k e^{j(n\theta_s + k\Omega t + k\lambda_k)} e^{-j(n+k)\theta_0} \quad (21)$$

For the k^{th} current harmonic, not all winding function n^{th} harmonics generate flux in the airgap, and the term $\sum_{\theta_0} e^{-j(n+k)\theta_0}$ inside (21) determines which harmonics generate flux.

The same way as permanent magnet linked flux was calculated in (5), linked flux induced by a phase ph_1 in another phase ph_2 is calculated by integrating the product between flux density and winding function in the coil area, which is shown in (22).

$$\Psi_{ph_2}^{ph_1}(t) = \frac{L_s D_g}{2} \int_0^{2\pi} M_{ph_2}(\theta_s) \cdot B_g^{ph_1}(\theta_s, t) \cdot d\theta_s \quad (22)$$

By replacing (3) and (20) in (22), (23) is obtained. Note that the winding function appears twice in the expression. As all harmonics of the first must be multiplied by all harmonics of the second, n_1 and n_2 are used to differentiate both multiplied n^{th} winding function harmonics.

$$\Psi_{ph_2}^{ph_1}(t) = \frac{L_s D_g \mu_0}{16g} \cdot \int_0^{2\pi} \sum_{[n_1, n_2, k]=-\infty}^{\infty} \hat{M}_{n_1} \hat{M}_{n_2} \hat{I}_k \cdot e^{j((n_1+n_2)\theta_s + k\Omega t + k\lambda_k)} e^{-jn_2\theta_{0,ph_2}} e^{-j(n_1+k)\theta_{0,ph_1}} d\theta_s \quad (23)$$

To get a non-zero value in the integral, $n_2 = -n_1$ must be met, which is substituted in (23) to get (24). $n = n_1$ is used in this last equation.

$$\Psi_{ph_2}^{ph_1}(t) = \frac{L_s D_g \mu_0 \pi}{8g} \sum_{[n,k]=-\infty}^{\infty} \hat{M}_n^2 \hat{I}_k \cdot e^{jk(\Omega t + \lambda_k - \theta_{0,ph_1})} e^{jn(\theta_{0,ph_2} - \theta_{0,ph_1})} \quad (24)$$

When it comes to the total flux generated by the stator armature and linked in each phase, the sum of all flux generating phases (ph_1) in (24) must be performed, obtaining (25).

$$\Psi_{ph}^s(t) = \frac{L_s D_g \mu_0 \pi}{8g} \sum_{[n,k]=-\infty}^{\infty} \hat{I}_k e^{jk(\Omega t - \theta_{0,ph} + \lambda_k)} \hat{M}_n^2 \sum_{\theta_0} e^{j(n+k)(\theta_{0,ph} - \theta_0)} \quad (25)$$

As regards the inductance, it relates the current with the generated flux as in (26).

$$L = \frac{\Psi(t)}{I(t)} \quad (26)$$

By applying this relationship to current and flux formulas in (11) and (24), and substituting $\theta_{0,ph_1} = \theta_{0,ph_2} = \theta_{0,ph}$, the self-inductance in a given phase ph can be calculated as in (27).

$$L_{ph} = \frac{L_s D_g \mu_0 \pi}{4g} \sum_{n=-\infty}^{\infty} \hat{M}_n^2 \quad (27)$$

Besides, the inductance value can also be calculated accounting with the flux created by all the stator coils, which is more interesting for motor control purpose. This way, for an m -phase motor with θ_0 phase shifts, the inductance for k^{th} current harmonic is calculated in (28),

$$\begin{aligned} L_k &= \frac{L_s D_g \mu_0 \pi}{4g} \sum_{n=-\infty}^{\infty} \hat{M}_n^2 \sum_{\theta_0} \left(e^{j(n+k)\theta_0} + e^{j(n-k)\theta_0} \right) \\ &= \frac{L_s D_g \mu_0 \pi}{g} \sum_{n=1}^{\infty} \hat{M}_n^2 \cdot c_L(n, k) \end{aligned} \quad (28)$$

where c_L follows the expression in (29).

$$c_L(n, k) = \sum_{\theta_0} \frac{\cos((n+k)\theta_0) + \cos((n-k)\theta_0)}{2} \quad (29)$$

Unlike the self-inductance, this time not all winding function harmonics affect the inductance value. Furthermore, the inductance for each k^{th} current harmonic is different and depends on the term $c_L(n, k)$.

IV. RESULTS AND DISCUSSION

To discuss about multiphase motors in this section, the DTP motor has been selected ($\theta_0 = [0, \frac{\pi}{6}, \frac{2\pi}{3}, \frac{5\pi}{6}, \frac{4\pi}{3}, \frac{3\pi}{2}]$). This is compared with the three-phase motor ($\theta_0 = [0, \frac{2\pi}{3}, \frac{4\pi}{3}]$).

A. Average torque

To get an average torque value, the term $e^{j(n+k)\Omega t}$ must be 1 in (14). Therefore, $n = -k$ must be substituted there to obtain the expression in (30).

$$T_{em,av}^{pm-s}(t) = \frac{L_s D_g \pi}{8} \sum_{k=-\infty}^{\infty} k \hat{M}_k \hat{B}_{gk} \hat{I}_k e^{j(\frac{\pi}{2} - k\lambda_k)} \quad (30)$$

The maximum value for average torque for the harmonic k is obtained when $\lambda_k = \frac{\pi}{2k}$ and \hat{I}_k has a positive value (assuming that the product $\hat{M}_k \cdot \hat{B}_{gk}$ has also a positive value), which allows to equal the exponential term in (30) to 1. Moreover, a high \hat{M}_k , \hat{B}_{gk} and \hat{I}_k produce a higher torque, which makes it interesting to have a high fundamental winding factor (\hat{M}_k) and airgap flux density (\hat{B}_{gk}) if high torque is required.

To sum up, k^{th} magnet flux density harmonic is linked by means of k^{th} winding factor harmonic, achieving an k^{th} EMF harmonic. By applying a same-order k^{th} current harmonic, average torque is achieved. The harmonic combinations that produce an average torque are marked in green in Fig. 2.

B. Torque ripple

The term $e^{j(n+k)\Omega t}$ appears in the torque expression. In the case of harmonics that do not match the equality $n = -k$, they produce an oscillating torque component. Whether torque ripple is created or not depends on the term $\sum_{\theta_0} e^{-j(n+k)\theta_0}$ which, in case of being null, eliminates the oscillating torque component.

In case of three-phase motors and considering that n and k are odd numbers, torque ripple appears when $n+k$ is a multiple of 6. The harmonic combinations that produce torque ripple (e.g. $k = 1$ and $n = 5$) are marked in red with a cross in Fig. 2a.

For higher number of phases, in m phase motors, the first component of torque ripple appears at $2m$ (except from symmetrical even phase number configurations, where it appears at m) which can be deduced from the mentioned term $\sum_{\theta_0} e^{-j(n+k)\theta_0}$. This means that the more phases has a motor, the smaller is the torque ripple, as more components are canceled in the expression. The specific case of the DTP motor is depicted in Fig. 2b. The sum $n+k$ must be multiple of 12 (e.g. $k = 1$ and $n = 11$), and the harmonic combinations are marked in red with a cross.

C. Current harmonic injection

To use additional current harmonics together with the fundamental one is possible in multiphase motors, which is called current harmonic injection (CHI) in the literature [12]. In a three-phase motor, the only harmonic that produces an average torque without ripples is the first one, and this scenario is depicted in Fig. 2a. In multiphase motors, additional current harmonics can be used to generate torque.

The case of the DTP motor can be analysed in Fig. 2b. If only the fundamental current harmonic is used, the 9th and lower-order EMF harmonics do not produce torque ripple.

value is required in the application (to improve power factor), as the remaining inductance not only behaves as a leakage inductance but also generates torque ripple. This ratio between the effective inductance and the total inductance for a given current harmonic is called in [13] the harmonic leakage factor.

V. FINITE ELEMENT COMPARISON FOR MODEL AND RESULTS VERIFICATION

In Section IV, the dissimilarities between 3-phase and multiphase motors were discussed. To further confirm the mentioned differences, FEM was used in both motor types. This way, the model and the results were verified. The ideal 3-pole-pair three-phase and DTP surface permanent magnet motors in Fig. 3 were selected, whose main dimensions and parameters are given in Table III. To make the motor ideal, the coils were represented as line regions to avoid the slotting effect. When it comes to the phase current value, 20 A and 10 A peak current values were used in the 3-phase and DTP motors respectively (same total ampere-turns).

A. Airgap flux generation

To analyse the airgap flux generated by the windings, magnets were defined as air in the FEM models. The airgap flux density created by the three-phase and the DTP motors can be appreciated in Fig. 4. The DTP motor generated a higher fundamental harmonic, which led to a higher average torque. Moreover, the 5th and 7th flux density harmonics did not appear in the DTP motor as predicted in Table II.

When feeding the DTP motor with different current harmonics, different winding function harmonics took part in generating airgap flux. This is illustrated in Fig. 5.

First, when feeding the motor with the 1st current harmonic, harmonics of electrical order $k = 12h \pm 1$ (where $h = 0, 1, 2, 3, \dots$) appeared. Second, when fed with the 5th current

TABLE III: Motor dimensions and parameters.

Parameter	Value	Parameter	Value
Rotor lamination radius	41 mm	Coil span	5°
Magnet length	1 mm	Magnet remanent flux density	1.2 T
Airgap length	0.1 mm	Magnet relative permeability	1
Axial length	36 mm	Steel relative permeability	$10^6 \approx \infty$
		Number of turns per phase	120

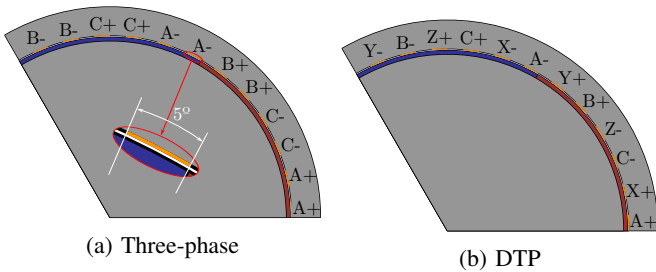


Fig. 3: Single pole pair of the selected motors for model and results verification.

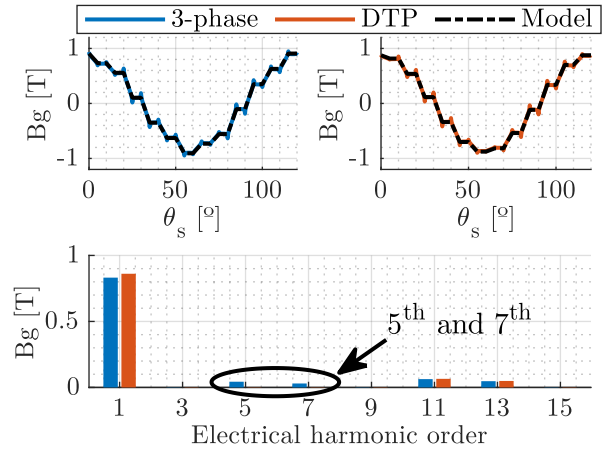


Fig. 4: Airgap flux density of three-phase and DTP motors without magnets.

harmonic, airgap flux harmonics of order $k = 12h \pm 5$ (where $h = 0, 1, 2, 3, \dots$) appeared. These results also match with Table II and graphically show the existence of the different inductances.

B. Torque generation

To compare both motors in terms of torque generation, they were fed with the same total ampere-turns. Fig. 6 shows the temporal waveforms and the Fast Fourier Transform (FFT).

When it comes to the average torque value, it was 3.5% higher in the DTP motor. This was due to the higher fundamental airgap flux generated by the stator winding, which was shown in Fig. 4.

Besides, torque ripple was considerably higher in the three-phase motor (15.3% in 3-phase and 3.4% in DTP peak-to-peak

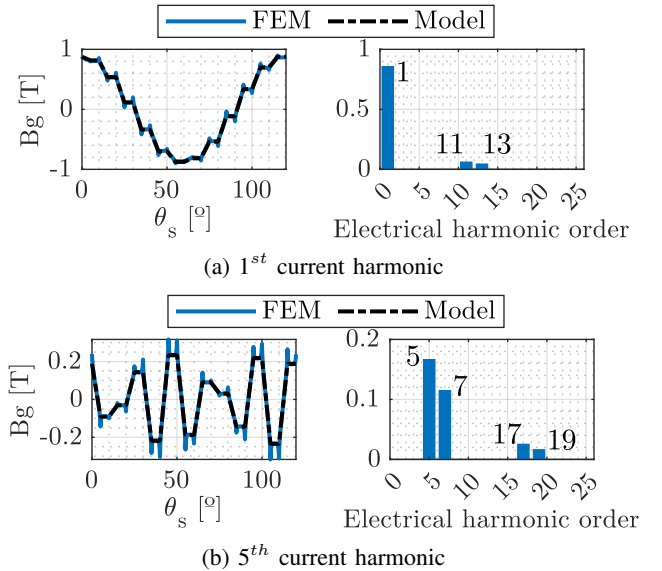


Fig. 5: Airgap flux density created by different current harmonics in the DTP motor without magnets.

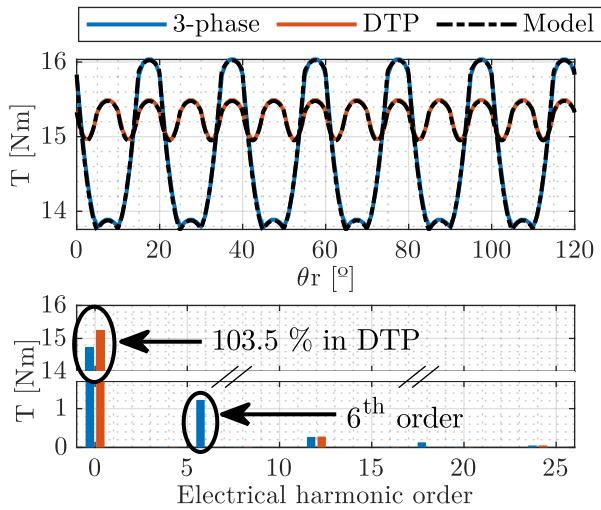


Fig. 6: Torque ripple in the three-phase and DTP motors at the same load point.

with respect to average value). The harmonics of electrical order 5 and 7 generated 6th electrical order torque ripple in the 3-phase motor as previously discussed in Section IV-B. In the case of the DTP motor, only harmonics of electrical order 12 and multiples appeared.

VI. CONCLUSIONS

The aim of this investigation was to develop a model to understand the different harmonic planes, inductances and torque generation in multiphase motors. The results of this study show the effects that the interaction of different harmonics have on inductance values and torque generation. This could help to improve motor designs, specially in the preliminary design stage due to the taken assumptions. The current study was limited by the fact that it did not take into account non-idealities of the motor, including saturation and reluctance. Considering non-idealities in the model as well as using it to analyse other motor topologies (e.g. concentrated winding designs) would be fruitful areas for further work.

REFERENCES

- [1] M. A. Frikha, J. Croonen, K. Deepak, Y. Benômar, M. El Baghdadi, and O. Hegazy, "Multiphase Motors and Drive Systems for Electric Vehicle Powertrains: State of the Art Analysis and Future Trends," *Energies*, vol. 16, no. 2, p. 768, jan 2023. [Online]. Available: <https://www.mdpi.com/1996-1073/16/2/768>
- [2] F. Barrero and M. J. Duran, "Recent Advances in the Design, Modeling, and Control of Multiphase Machines—Part I," *IEEE Transactions on Industrial Electronics*, vol. 63, no. 1, pp. 449–458, jan 2016. [Online]. Available: <http://ieeexplore.ieee.org/document/7128683/>
- [3] X. Kestelyn and E. Semail, "Vectorial Modeling and Control of Multiphase Machines with Non-salient Poles Supplied by an Inverter," in *Control of Non-conventional Synchronous Motors*, J.-P. Louis, Ed. Wiley, jan 2012, ch. 5, pp. 161–206. [Online]. Available: <https://onlinelibrary.wiley.com/doi/10.1002/9781118603208.ch5>
- [4] A. Tassarolo, L. Branz, and M. Bortolozzi, "Stator inductance matrix diagonalization algorithms for different multi-phase winding schemes of round-rotor electric machines part I. theory," in *IEEE EUROCON 2015 - International Conference on Computer as a Tool (EUROCON)*. IEEE, sep 2015, pp. 1–6. [Online]. Available: <http://ieeexplore.ieee.org/document/7313776/>

- [5] —, "Stator inductance matrix diagonalization algorithms for different multi-phase winding schemes of round-rotor electric machines part II. Examples and validations," in *IEEE EUROCON 2015 - International Conference on Computer as a Tool (EUROCON)*. IEEE, sep 2015, pp. 1–6. [Online]. Available: <http://ieeexplore.ieee.org/document/7313777/>
- [6] F. Scuiller, E. Semail, and J.-F. Charpentier, "General modeling of the windings for multi-phase ac machines - Application to the analytical estimation of the mutual stator inductances for smooth air gap machines," *Eur. Phys. J. Appl. Phys.*, vol. 50, no. 3, p. 31102, 2010. [Online]. Available: <https://doi.org/10.1051/epjap/2010058>
- [7] A. Tassarolo, "Accurate Computation of Multiphase Synchronous Machine Inductances Based on Winding Function Theory," *IEEE Transactions on Energy Conversion*, vol. 27, no. 4, pp. 895–904, dec 2012. [Online]. Available: <http://ieeexplore.ieee.org/document/6317162/>
- [8] I. Eguren, G. Almandoz, A. Egea, X. Badiola, and A. Urdangarin, "Understanding Switched-Flux Machines: A MMF-Permeance Model and Magnetic Equivalent Circuit Approach," *IEEE Access*, vol. 10, pp. 6909–6928, 2022. [Online]. Available: <https://ieeexplore.ieee.org/document/9672124/>
- [9] G. Almandoz, J. Poza, M. A. Rodriguez, and A. Gonzalez, "Analytic model of a PMSM considering spatial harmonics," in *2008 International Symposium on Power Electronics, Electrical Drives, Automation and Motion*. IEEE, jun 2008, pp. 603–608. [Online]. Available: <http://ieeexplore.ieee.org/document/4581080/>
- [10] A. Egea, G. Almandoz, J. Poza, and A. Gonzalez, "Analytic model of axial flux permanent magnet machines considering spatial harmonics," in *SPEEDAM 2010*. IEEE, jun 2010, pp. 495–500. [Online]. Available: <http://ieeexplore.ieee.org/document/5542393/>
- [11] V. Kindl, R. Cermak, Z. Ferkova, and B. Skala, "Review of Time and Space Harmonics in Multi-Phase Induction Machine," *Energies*, vol. 13, no. 2, p. 496, jan 2020. [Online]. Available: <https://www.mdpi.com/1996-1073/13/2/496>
- [12] Y. Hu, K. Huang, X. Li, D. Luo, S. Huang, and X. Ma, "Torque enhancement of dual three-phase PMSM by harmonic injection," *IET Electric Power Applications*, vol. 14, no. 9, pp. 1735–1744, sep 2020. [Online]. Available: <https://onlinelibrary.wiley.com/doi/10.1049/iet-eap.2019.0882>
- [13] S. Skoog and A. Acquaviva, "Pole-Slot Selection Considerations for Double Layer Three-phase Tooth-Coil Wound Electrical Machines," in *2018 XIII International Conference on Electrical Machines (ICEM)*. IEEE, sep 2018, pp. 934–940. [Online]. Available: <https://ieeexplore.ieee.org/document/8506772/>

VII. BIOGRAPHIES

Beñat Arribas received his B.Sc. degree in electronics engineering in 2020 and the M.Sc. degree in energy and power electronics in 2022, both from Mondragon Unibertsitatea, where he is currently pursuing the PhD degree. His current research interests include electrical machine analysis and design.

Aritz Egea received the degree in electrical engineering in 2009 and the PhD degree in electrical engineering in 2012, both from the Mondragon Unibertsitatea, where he is currently an Associate Professor. His current research interests include electrical machines and electromagnetic actuators.

Gaizka Almandoz (M'04) received the B.Sc. and PhD degrees in electrical engineering from Mondragon Unibertsitatea in 2003 and 2008, respectively, where he is currently an Associate Professor. His current research interest includes electrical machine design, modelling, and control.

Javier Poza received the B.S. degree in Electrical Engineering from Mondragon Unibertsitatea, in 1999 and the Ph.D. degree in electrical engineering from the Institut National Polytechnique de Grenoble, France. Since 2002, he is an Associate Professor in Mondragon Unibertsitatea. His current research interests include electrical machine design, modelling, diagnostic and control.

Ion Iturbe is a Doctor in Electrical engineering by the Institut National Polytechnique de Grenoble (INPG). During 10 years worked in the modeling and control of magnetically levitated systems and in system automation in a R&D center. Since 2020, he works as researcher-professor at Mondragon Unibertsitatea, in the field of modeling and control of electric drives.